J. Sens. Sens. Syst., 3, 177–185, 2014
www.j-sens-sens-syst.net/3/177/2014/
doi:10.5194/jsss-3-177-2014

JSSS Journal of Sensors and Sensor Systems Open Access

Humidity measurement with capacitive humidity sensors between −70 °C and 25 °C in low vacuum

A. Lorek

German Aerospace Center (DLR), Berlin, Germany

Correspondence to: A. Lorek (andreas.lorek@dlr.de)

Received: 28 December 2013 – Revised: 24 June 2014 – Accepted: 9 July 2014 – Published: 29 August 2014

Abstract. At the German Aerospace Center (DLR), capacitive humidity sensors are used to measure relative humidity in experiments under extreme atmospheric conditions such as on Mars or in the coldest regions on Earth. This raises the question whether such experiments can be performed using low-cost humidity sensors with a tolerable measurement uncertainty. As part of the standardizing project SMADLUSEA (project no. SF11021A), nine capacitive humidity sensors (Sensirion SHT75) were investigated for pressure ranging from 10 to 1000 hPa (low vacuum) and temperatures from −70 to 25 °C. It has been shown that these sensors worked reliably and with reproducibly measured values over the entire investigated pressure and temperature range. There was no aging of the sensors observable. In addition to the known strong temperature dependency, the SHT75 also shows a pressure dependency below −10 °C. A characteristic curve for the SHT75 was calculated with an expanded uncertainty of 7 % of the measured values.

In conclusion, low-cost capacitive humidity sensors offer the option to obtain reliably measured values even under extreme conditions with comparatively little effort.

1 Introduction

What are the most useful sensor principles and their potential measurement ranges under Martian conditions? This was a fundamental question for the development of the in situ trace humidity measuring system called MiniHUM, designed for the ExoMars lander to measure the humidity of the near-surface Martian atmosphere (Koncz, 2012). The coulometric and capacitive sensor principles were chosen to develop a lightweight and low-energy device. The coulometric sensors (Lorek et al., 2010), which we will not further described in this paper, measure the absolute humidity and have the potential to detect trace humidity below frost points of −100 °C. However, our own measurements have shown low chemical activity at temperatures less than −50 °C which leads to a limited functionality for this type of sensor.

At standard environmental conditions (25 °C and 1013 hPa), the capacitive sensors measure reliably in the range from 10 to 90 % relative humidity ($U_{w,i}$). However, there are only insufficient data, even for coulometric sensors, about the behavior in low vacuum (1 to 1000 hPa) and temperatures between −70 and 25 °C. Evidence for the ability of the capacitive sensor principle is the Phoenix Mars mission (Zent et al., 2010). Capacitive humidity sensors are also used successfully in meteorology, for example, on radiosondes in weather balloons. While some of them have been investigated for temperatures down to −70 °C (Miloshevich et al., 2001; Hudson et al., 2004), there are not sufficient data on their behavior in a low vacuum especially down to 10 Pa.

Our measurements of nine capacitive humidity sensors type SHT75 from Sensirion AG (2011) provide a database which demonstrates function and measurement uncertainty of off-the-shelf sensors in the already mentioned pressure and temperature range. The experiments were performed at the Martian Simulation Facility (MSF) at DLR (Lorek and Koncz, 2013).

2 Theoretical background

The SHT75-sensors measure the relative humidity $U_{w,i}$ (Eq. 1), defined as the ratio in per cent of the water vapor partial pressure e [Pa] to saturation vapor pressure under

saturation conditions above a planar water e_w [Pa] or ice surface e_i [Pa] at the same total pressure p [Pa] and temperature T [K] (derived from WMO, 2012):

$$U_{w,i} = \left(\frac{e}{e_{w,i}}\right)_{p,T} 100\,\%. \quad (1)$$

In this paper conditions of pure phase e were assumed and used for calculations and not the water vapor partial pressure in a real gas e', because the difference between both pressures is $< 0.5\,\%$ and negligible for this investigation (VDI/VDE 3514 Part 1, 2007; Bögel, 1977; WMO, 2012).

The following Eqs. (2) for e_w [hPa] and (3) for e_i [hPa] are recommended by WMO (2012). Equation (2) is related within the temperature range from −50 to 100 °C

$$\begin{aligned}\lg e_w = {} & 10.79574\left(1-\frac{T_1}{T}\right) 5.028 \lg\left(\frac{T_1}{T}\right) \\ & + 1.50475\times10^{-4}\left[1-10^{-8.2969\left\{\frac{T}{T_1}\right\}}\right] \\ & + 0.42873\times10^{-3}\left[10^{+4.76955\left\{1-\frac{T}{T_1}\right\}}-1\right] \\ & + 0.78614 \end{aligned} \quad (2)$$

and Eq. (3) from −100 to 0 °C with $T_1 = 273.16$ K (triple point temperature of water):

$$\begin{aligned}\lg e_i = {} & -9.09685\left(\frac{T_1}{T}-1\right) - 3.56654\lg\left(\frac{T_1}{T}\right) \\ & + 0.87682\left(1-\frac{T_1}{T}\right) + 0.78614. \end{aligned} \quad (3)$$

The WMO (2012) recommends calculating the relative humidity relative to U_w. One reason is that for temperatures below 0 °C, the relative humidity in clouds is often supersaturated with respect to ice ($U_i > 100\,\%$). A further reason is a better comparability of the most meteorological measurements witch are often displayed in U_w.

However, the measurements discussed in this paper were partially performed down to −70 °C. This is out of the range of Eq. (2). A super-saturation of the sample gas seems to be unlikely because there are enough inner surfaces in pipes and measurement cells for the condensation of surplus water vapor. Therefore, in this paper, the relative humidity below 0 °C is obtained in relation to ice (U_i) according to the technical definition for the relative humidity (VDI/VDE 3514 Part 1, 2007).

3 Experimental procedure

3.1 Experimental setup

3.1.1 Sensors and measured value acquisition

The investigated SHT75 is a polymer based capacitive humidity sensor manufactured in CMOS technology. In addition it has a band-gap temperature sensor and electronic units for signal processing (Sensirion AG, 2011). The humidity sensor measures the permittivity of the hydrophilic polymer depending of the adsorbed water content which is affected by the partial water vapor pressure of the surrounding atmosphere. An integrated A/D converter generates a serial output from the analog measurement signal at the digital interface. The dimensions without electrical connectors are $(6.4 \times 3.7 \times 3.1)$ mm (length × width × height).

A nine-channel measuring device for SHT sensors from dr. wernecke Feuchtemesstechnik GmbH was used to process the serial data and output an integer rough humidity value (SO_{RH}) and temperature value. From these, the device calculates the relative humidity value $U_{w(SHT75)}$, based on Eq. (4).

The measuring range for U_w specified by the manufacturer is from 0 to 100 % and for the temperature from −40 to 123.8 °C.

Equation (4) is the manufacturer formula (Sensirion AG, 2011) for the calculation of the temperature compensated relative humidity:

$$\begin{aligned} U_{w(SHT75)} = {} & (t-25)\,(0.01 + 0.00008 SO_{RH}) \\ & - 2.0468 + 0.0367 SO_{RH} \\ & - 1.5955\times10^{-6} SO_{RH}^2 \end{aligned} \quad (4)$$

using t [°C] as sensor temperature.

The expanded uncertainties (U_{99}) for $U_{w(SHT75)}$ is $U_{99} = 1.8\,\%$ within U_w 10 to 90 % at 25 °C and increase to the measuring range limits of $U_{99} = 4\,\%$. The expanded uncertainty for the temperature increases from $U_{99} = 0.3$ K at 25 °C to a maximum of 1.5 K at −40 °C (Sensirion AG, 2011).

The expanded uncertainties U_{99}, given in this paper, result from a multiplication of the standard uncertainty u (type A or B) with factor of 3 ($k = 3$) and include 99 % of the measured values (GUM, 2008).

Using SHT75 has an historical background. To measure in situ the near-surface atmospheric humidity on Mars in 2003 our laboratory was looking for a humidity sensor. Information from the Open University about this sensor working under extreme conditions and its special features (e.g., digital output, low hysteresis, inexpensive, low power consumption, off-the-shelf product and certified) led to the choice of the SHT75. Since then, the laboratory has been using this sensor.

The investigated temperatures range down to −70 °C which is lower than the threshold of −40 °C for the SHT75 measuring range. Therefore and as a reference, 15 Pt100 temperature sensors were used. Twelve of them were Pt100 thin-film resistors 6W 538 from IST AG (2012) with the dimensions $5 \times 3.8 \times 0.65$ mm (length × width × height) and three were Pt100-wire-wound resistors from Service für Messtechnik Geraberg GmbH, all with classification A. The wire-wound resistors were cased in a copper block to prevent damage by the mounting on the exterior measuring cell housing. The block dimensions are $10 \times 3 \times 3$ mm (length × width × height). The Pt100 sensors were calibrated

for temperatures between −75 and 50 °C (Deep-Well-Bad 7831, Fluke Europe B.V) with a resulting expanded uncertainty for all Pt100 of $U_{99} = 0.1$ K.

The pressure measurement was done using an Active Capacitive Transmitter CMR 361 (Pfeiffer Vacuum GmbH). It has an effective range from 0.1 to 1100 hPa and an $U_{99} = 0.01$ % (full scale) in the range from 1 to 40 000 Pa and an $U_{99} = 0.1$ % for $p > 40\,000$ Pa.

A Keithley-digital multimeter DMM 3706 with integrated Dual 1 × 20 Multiplexer-card (Model 3721 with 3721-ST screw terminal) was used for data acquisition from CMR 361 and all Pt100.

A dew point mirror hygrometer S8000RS (Michell Instruments GmbH) was the reference for the humidity of the sample gas. It has a measuring range from ca. −100 °C frost point temperature (t_f) to 20 °C dew point temperature (t_p) with an expanded uncertainty of $U_{99} = 0.3$ K at 20 °C to 0.51 K at −60 °C.

3.1.2 Experimental setup

The experimental setup, basically described by Lorek and Koncz (2013), consists of a gas mixing system, a temperature test chamber which contains the measuring cells, a membrane vacuum pump (Fig. 1) and the measurement equipment mentioned in Sect. 3.1.1. The pipes, measuring cells and connection components between gas mixing system and vacuum pump consisted of stainless steel to minimize adsorption at and permeation through the pipe walls.

The sample gas can be nearly continuously humidified in an absolute humidity range from −73 °C (t_f) to 5 °C (t_p).

It was found that for the pipes which transport the sample gas inside the chamber to the measuring cells, a diameter of DN 16 is sufficient to ensure constant pressure and prevent water condensation in pipes and cells inside the chamber (Fig. 2). The dimensions of the measuring cells are 180 × 70 × 70 mm (length × width × height). Each cell has a centered 38 mm diameter hole over the entire length and two blind holes of the same dimensions down to the vertical center with a distance of 80 mm. These blind holes form the measuring chambers holding the sensors and exposing them to the sample gas (Fig. 2a).

3.1.3 Sensor setup

Each of the CF-DN40 flanges sealing the first measuring chamber of each measuring cell (Fig. 2) is equipped with a 2 mm stainless steel pipe for the pressure measurement and a 32-pin male connector. Both were glued into the flange using ECCOBOND 286 (2013). The connectors provide the electrical feedthrough for 4 Pt100 (four-wire configuration) and three SHT75 on each measuring cell.

The SHT75 measurement range for temperature is limited at −40 °C. Therefore, a calibrated Pt100 was glued onto each SHT75 (Sect. 3.1.1). The fourth Pt100 was placed in

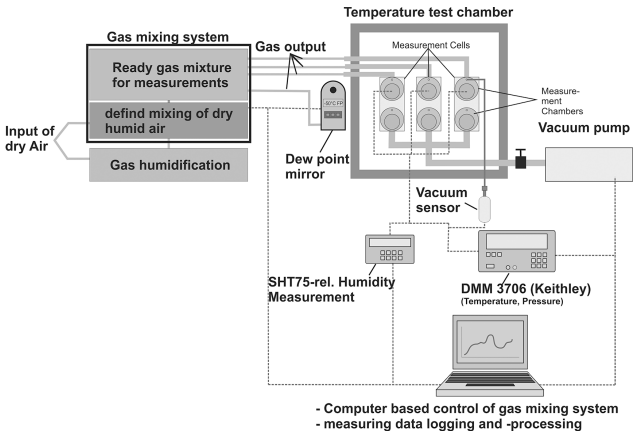

Figure 1. Experimental setup.

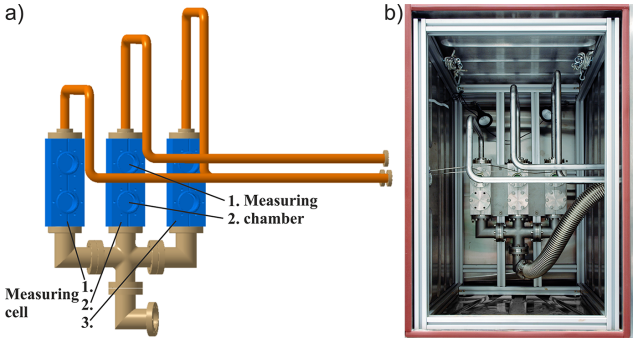

Figure 2. **(a)** Illustration of measuring cells and pipe routing inside the temperature test chamber; **(b)** temperature test chamber with measuring cells.

the center of the three mounted SHT75/Pt100 combinations (Fig. 3). This Pt100 measured the undisturbed gas temperature to reveal temperature differences between the Pt100–SHT75 combinations and the housing temperature. In order to place sensors in the center of the gas flow, they were soldered to the connector with 15 mm enameled copper wires (diameter 150 µm).

A 1.8 m four-wire cable with PFA-coating (usable down to −200 °C) was used to connect each sensor with the measurement device. To minimize heat influences from the outside, cables were routed mainly inside the temperature test chamber. Finally, for every measuring cell, one Pt100 (Sect. 3.1.1) was mounted outside every measurement cell to measure the housing temperature.

The quantity of nine SHT75 is given by the Pt100 measuring equipment and the selected 32-pin male connector.

In the following each SHT75 and Pt100 will be designated using the nomenclature in Table 1.

Table 1. Nomenclature for the Pt100 and SHT75 used.

Nomenclature	SHT75	Pt100 at SHT75	Pt100 in the middle	Measuring cell Pt100 outside at
Measuring cell 1	SHT75_1 SHT75_2 SHT75_3	Z1PtS1 Z1PtS2 Z1PtS3	Z1Pt1	Z1B1
Measuring cell 2	SHT75_4 SHT75_5 SHT75_6	Z2PtS1 Z2PtS2 Z2PtS3	Z2Pt1	Z2B1
Measuring cell 3	SHT75_7 SHT75_8 SHT75_9	Z3PtS1 Z3PtS2 Z3PtS3	Z3Pt1	Z3B1

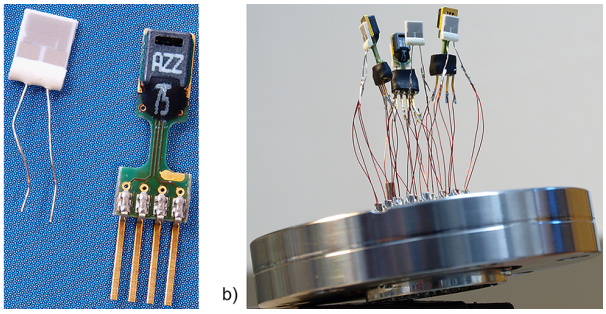

Figure 3. **(a)** Left: Pt100 (6W 538), and right: SHT75; **(b)** three SHT75/Pt100 combinations with the fourth Pt100 placed in the center.

3.2 Experimental procedure

After a leakage test, a continuous volume flow of $\dot{V}_N = 30\,\mathrm{L\,h^{-1}}$ (at 20 °C and 1013 hPa) sample gas was passed through each cell (Figs. 1 and 2a). At 10 hPa, the flow has to be reduced to $\dot{V}_N = 15\,\mathrm{L\,h^{-1}}$ to ensure not to exceed the performance of the vacuum pump. When at the required temperature thermal equilibrium was reached inside the measuring chamber, the measurements were started at the highest pressure for this temperature (Table 2) and, if possible, the relative humidity steps between $U_{\mathrm{w,i(ref)}}$ ca. 5 and 95 % were generated. The achievable relative humidity was limited due to the chamber temperature and the generated humidity of the gas mixing system. The pressure was kept constant over 0.5 to 15 h depending on the expected duration to reach humidity equilibrium at each humidity step of the measuring chambers and sensors.

The investigated temperatures, pressures and relative humidities are listed in Table 2. The calculation of the relative reference humidity $U_{\mathrm{w,i(ref)}}$ inside the measuring chambers using Eq. (1) is based on the assumption that

$$\frac{e_{\mathrm{ref}}}{e_{(\mathrm{ref}N)}} = \frac{p}{p_N} \quad \text{and thereby}$$

Table 2. Range of the relative humidity under investigation for the different temperature and pressure conditions. Relative humidity is calculated with respect to water U_{w} or ice U_{i} (marked by brackets).

	P in hPa					
	1000	800	500	200	100	10
25 °C	28 2	18 3	11 4	4		
10 °C	71 1	57 4	36 4	14 5	7	
0 °C	91 6	89 6	72 6	29 5	14 5	
−10 °C	90 (99) 5 (6)	88 (97) 5 (6)	84 (93) 5 (6)	62 (68) 5 (6)	29 (32) 5 (6)	4 (5)
−20 °C	79 (96) 4 (5)	79 (96) 5 (6)	82 (100) 4 (5)	77 (94) 4 (5)	66 (79) 5 (6)	7 (9) 4 (5)
−30 °C	74 (99) 4 (5)	74 (99) 4 (5)	74 (99) 4 (5)	74 (99) 4 (5)	66 (89) 3 (4)	18 (24) 3 (4)
−40 °C	65 (96) 7 (10)	55 (81) 6 (9)	67 (99) 3 (4)	67 (98) 3 (4)	60 (89) 3 (4)	53 (78) 3 (4)
−50 °C	(85) (5)		(93) (7)	(93) (14)	(89) (20)	(99) (8)
−60 °C	(75) (10)		(71) (5)	(90) (17)		(99) (17)
−70 °C			(86) (18)	(79) (14)		(99) (15)

$$U_{\mathrm{w,i(ref)}} = \left(\frac{e_{\mathrm{ref}}}{e_{\mathrm{w,i}}}\right)_{\mathrm{p},T} 100\,\%, \tag{5}$$

where $e = e_{\mathrm{ref}}$ is the partial water vapor pressure inside the measuring chamber and $e_{(\mathrm{ref}N)}$ is the partial water vapor pressure at normal pressure p_N [101 325 Pa]. Depending on the $t_{\mathrm{p,f}}$ values given by the dew point hygrometer and the measured values p from the vacuum sensor CMR 361 (Sect. 3.1.1, Fig. 1), the value $e_{(\mathrm{ref}N)}$ was calculated from Eqs. (2) or (3).

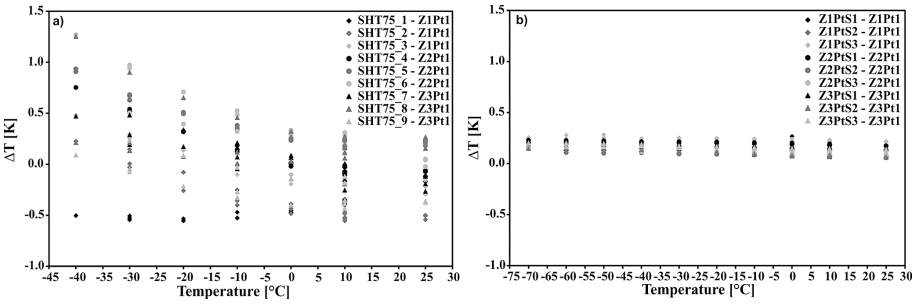

Figure 4. ΔT of the measured values relative to the Pt100 in the middle of each measuring chamber. In **(a)** temperature is measured by the Pt100 glued onto SHT75, while in **(b)** temperature is measured by the SHT75 itself.

3.3 Experimental results

3.3.1 Temperature

Figure 4 shows the average values of the temperature differences (ΔT), calculated from the measurements of the Pt100 glued onto the SHT75 (see Table 1, column 3, and Fig. 3b) and the SHT75 temperature values relative to the Pt100 placed in the center (see Table 1, column 4, and Fig. 3b) at each temperature (see Table 2, column 1). The expanded uncertainty of ΔT is in Fig. 4a $U_{99} = 0.32$ K at 25 °C to $U_{99} = 1.5$ K at −40 °C and in Fig. 4b $U_{99} = 0.15$ K.

Figure 4a shows the aberration development for the SHT75 band-gap temperature sensors from 0.5 K at 25 °C to 1.3 K at −40 °C. This increase of aberration to the Pt100 reference is due to the reduction of accuracy at low temperatures (Sensirion AG, 2011).

Figure 4b shows clearly that the temperature measurement with Pt100 compared to the measurement with the SHT75 band-gap temperature sensor (Fig. 4a) leads to a significantly smaller and temperature-independent variability of the measured values. This has a direct influence on the precision and accuracy of the relative humidity measurements. The observable offset of ca. 0.2 K in Fig. 4b probably results from the emitted heat of the active SHT75 (see Sensirion AG, 2011) and is, due to the strong scattering of the ΔT values, in Fig. 4a not clearly observable.

A comparison of the temperature measured by the Pt100 mounted outside the cells (see Table 1, column 5) with the Pt100 placed in the center (see Table 1, column 4) shows nearly identical temperature values with deviations within the uncertainty of the measurement (see Sect. 3.1.1). Therefore, it can be assumed that the sample gas temperature was identical to the cell housing temperature and that the active SHT75 sensors indeed generate the temperature increase of 0.2 K.

3.4 Relative humidity

In Fig. 5a–d, we show the signal of the SHT75_5 (see Table 2) representative for the other eight SHT75. $U_{w(SHT75)}$ was calculated from Eq. (4) based on the temperature and humidity measurements of the SHT75 and $U_{w(ref)}$ from Eqs. (2) and (5) based on the $t_{p,f}$ values of the dew point hygrometer and the measurements of the Pt100 glued onto the SHT75 (see Table 1, column 3). Note that the U_w values for −70 °C in Fig. 5d lie outside the range of validity of Eq. (2) but these values are irrelevant for the demonstration of the reliability. The peaks in Fig. 5d result from the automatic calibration function of the dew point hygrometer. Temperature and pressure influence the sorption rate of water molecules at the sensors and at the walls of pipes and measuring cells. This effect changes the equilibration time of the entire experimental system. A comparison of the sensor response time ($T90$) of Fig. 5a with b at the same pressure of 1000 hPa shows a significant delay of some minutes at 10 °C and nearly an hour at −40 °C and therefore a strong dependency on temperature. For this reason, we did not perform measurements at −70 °C and 1000 hPa because the response time of the sensors for each humidity step would have required several days with a resulting increase of the scatter of the measured values and a decrease of the sensitivity (see the 500 hPa-fit in Sect. 3.4.3). The situation was different at lower pressure. A comparison at 1000 hPa (Fig. 5b) with 10 hPa (Fig. 5c) at −40 °C shows a reduction of the $T90$ time to < 10 min.

The nine SHT75 sensors were tested in several test series over 136 days. On 74 days of this time, the sensors were subjected to temperatures < −40 °C, which is outside their specifications (see Sect. 3.1.1). Nevertheless, the sensors were still functioning (Fig. 5d) and showed reproducible results (see Sects. 3.4.3 and 3.4.4) over the entire temperature and pressure range (Table 2).

3.4.1 Comparison with manufacturer's data of the SHT75

Figure 6 shows the $U_{w(SHT75)}$ values from Eq. (4) at temperatures between −40 and 10 °C and a pressure of 1000 hPa based only on SHT75 measurements. The calculation of $U_{w(ref)}$ has been described in Sect. 3.4. The area marked in grey illustrates the expanded uncertainty U_{99} calculated using the standard uncertainty (type B GUM, 2008) with the

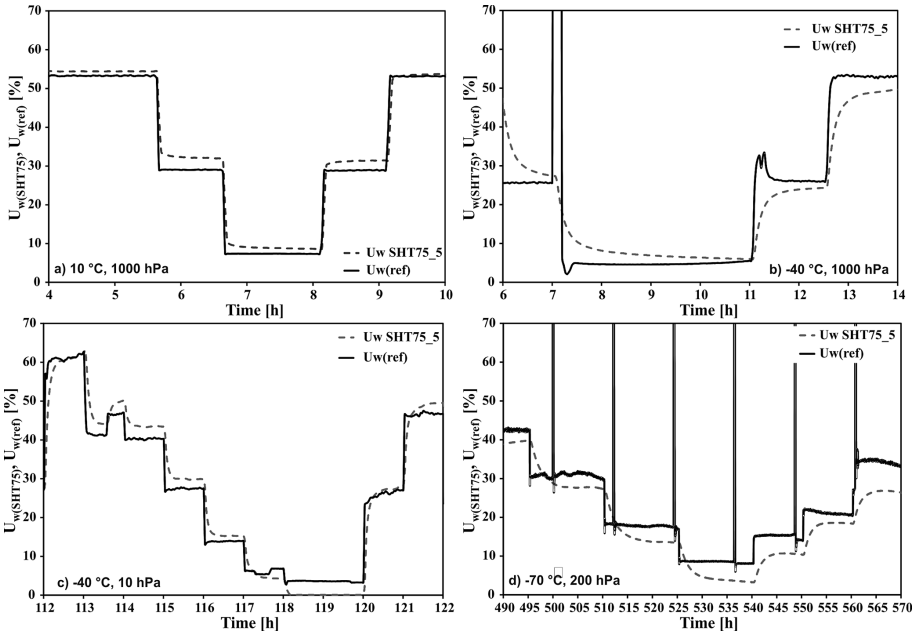

Figure 5. Signal of SHT75_5 (representative for all SHT75 sensors) at different temperatures and pressures.

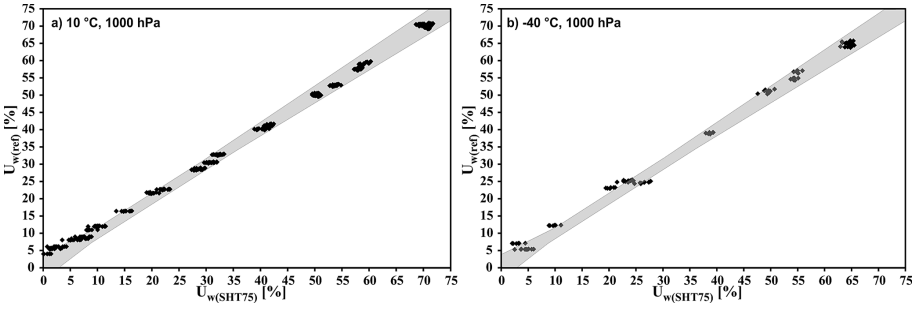

Figure 6. $U_{w(SHT75)}$ values of all SHT75 sensors at 1000 hPa for **(a)** 10 °C and for **(b)** −40 °C.

assumption that the measured values are normally distributed around the diagram diagonal.

For both temperatures, the expanded uncertainty of $U_{w(ref)}$ is $U_{99} = U_{w(ref)} \cdot 0.05$ and $U_{99} = 1.8\,\%$ for $U_{w(SHT75)}$ with an increase to 4 % at most for U_w at 0 or 100 % (see Sect. 3.1.1) were calculated based on the uncertainties for sensors and measuring instruments in Sect. 3.1.1.

The $U_{w(SHT75)}$ values in Fig. 6a are at $U_{w(ref)}$ values > 20 % within the calculated uncertainty area. Below this value, the measured $U_{w(SHT75)}$ values differ more and more to one side of the diagonal and partially are not inside the calculated uncertainty range. For −40 °C (Fig. 6b), a similar behavior with stronger variation can be observed. It appears that not all error sources of the measuring system are sufficiently known at lower humidity and temperatures to explain the observed systematic error. A leakage is unlikely because the $U_{w(SHT75)}$ values are lower than the $U_{w(ref)}$ values. Further possibilities are the inaccuracy of the manufacturer's fit or, more likely, deviations from this fit through gluing the

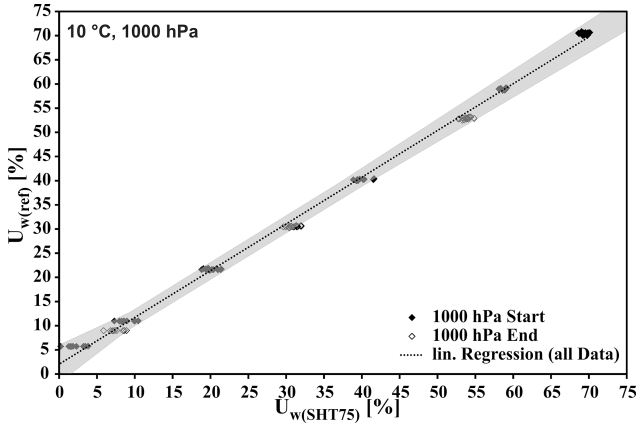

Figure 7. $U_{w(SHT75)}$ values at 10 °C and 1000 hPa of all SHT75 at the start and end of the 136 days test time; expanded uncertainty area marked in grey.

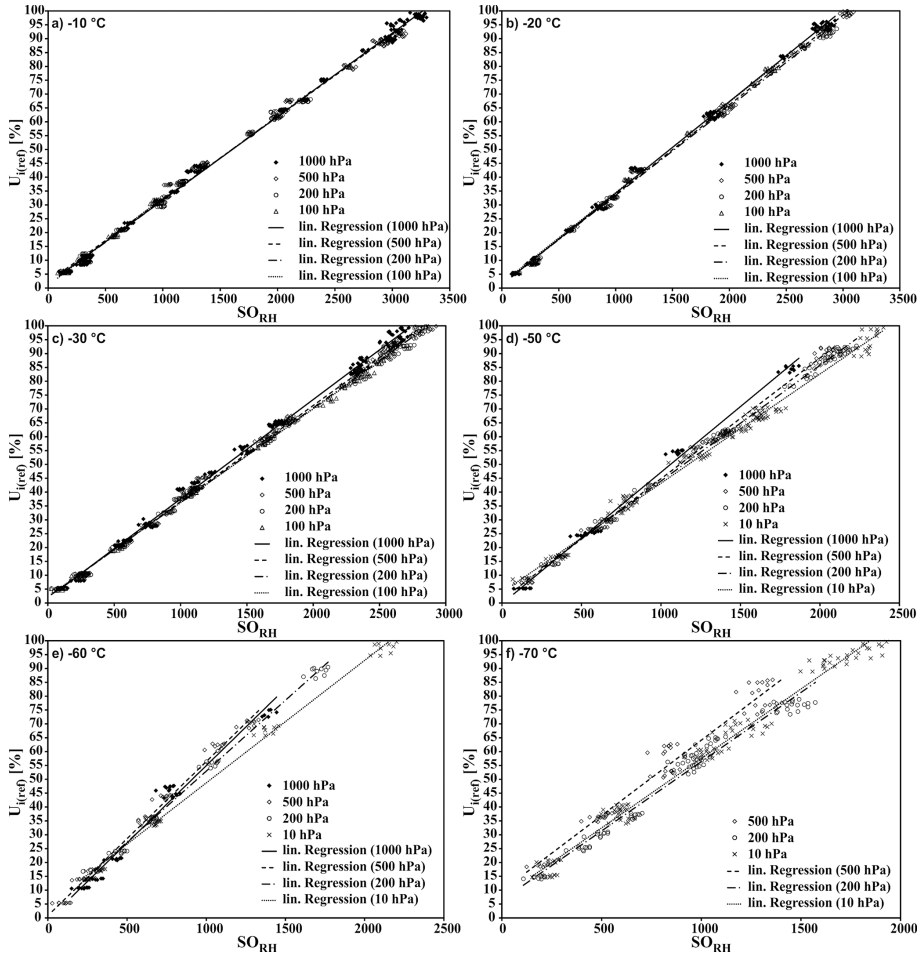

Figure 8. Pressure dependency of all SHT75 sensors at temperatures from −70 to −10 °C.

Pt100 onto the SHT75 (see Sect. 3.1.3). A final determination of the reason for the error is not possible because an unaltered SHT75 was not tested.

3.4.2 Aging of the SHT75

Figure 7 illustrates the $U_{w(SHT75)}$ values of all SHT75 at 10 °C and 1000 hPa at the start and end of the 136 day test time. The area marked in grey shows the expanded uncertainty from Sect. 3.4.1 but relative to the linear regression fit of the measurements rather than to the diagonal as in Fig. 6. Therefore, the systematic error (see Sect. 3.4.1) is included in the error analysis.

Even though the sensors were exposed to conditions beyond their specifications (see Sect. 3.1.1), for 74 days out of 136 days the $U_{w(SHT75)}$ values in Fig. 7 are mainly within the expected uncertainty. A drift in the measurements was not observed.

3.4.3 Pressure dependency of the SHT75

In this section, the relation of the SO_{RH} values (see Sect. 3.1.1) and $U_{i(ref)}$ values (see Sect. 3.4) is evaluated as a function of pressure.

We do not observe pressure dependence (Table 2) in the temperature range from −10 to 25 °C (see Fig. 8a). In the range from −20 to −50 °C (Fig. 8b to d), an increase of the scatter in the measurements as a function of increasing pressure was detected. At −60 °C (Fig. 8e), the regression fits of 1000 hPa, 500 hPa and 200 hPa are in better mutual agreement again. Only the 10 hPa fit differs clearly from the others. At −70 °C (Fig. 8f), a pressure dependence can no longer be observed. The deviation of the fit at 500 hPa is a result of the strong variation of the measured values which are located below the fit as the humidity is decreased and above the fit as the humidity is increased. This could be an indication of a hysteresis of the sensors caused by sorption behavior of the polymer and not by instability of the polymer under these extreme conditions because there is no drift at the pressure of 10 hPa observable (Fig. 8f) and no aging (see Sect. 3.4.2 and Fig. 7).

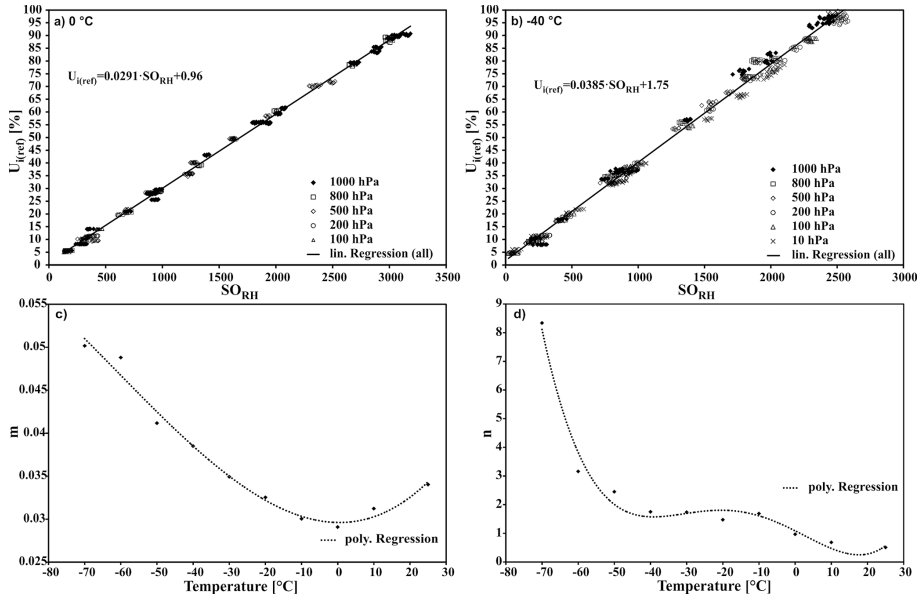

Figure 9. All SO_{RH} values of the nine SHT75 at **(a)** 0 °C and **(b)** −40 °C; **(c)** slope m and **(d)** offset n of the linear regression fit for all temperatures.

In general, the measurements showed a decrease in the equilibration times of the system with decreasing pressure and simultaneous increase of the sensitivity of the SHT75.

3.4.4 Temperature dependency of the SHT75

The SHT75 showed a strong temperature dependency of the SO_{RH} values which was also observed by the manufacturer (Sensirion AG, 2011). We perform a linear fit (see Fig. 9a, b)

$$U_{\mathrm{w,i(ref)}} = m\mathrm{SO_{RH}} + n \tag{6}$$

for the different temperatures under investigation (Fig. 9c, d). A polynomial fit performed for the data in Fig. 9c and d gives

$$m = 3.74557 \times 10^{-8} t^3 + 6.894 \times 10^{-6} t^2 - 6.42783 \times 10^{-6} t + 0.03 \tag{7}$$

$$n = 1.11357 \times 10^{-6} t^4 + 6.23536 \times 10^{-5} t^3 - 5.59115 \times 10^{-4} t^2 - 0.06308 t + 1.09. \tag{8}$$

Figure 10 shows the $U_{\mathrm{w,i(SHT75/Pt100)}}$ values calculated from Eqs. (6)–(8) based on all SO_{RH} values, measured at the temperatures and pressures listed in Table 2. In the calculation, the temperature values of the Pt100 glued onto the SHT75 (see Table 1, column 3) were used. The expanded uncertainty of $U_{\mathrm{w,i(SHT75/Pt100)}}$ and $U_{\mathrm{w,i(ref)}}$ is $U_{99} = 7\,\%$ (grey area in Fig. 10). The statistical error analysis is based on Hässelbarth (2004) for a linear calibration of type A (GUM, 2008). The values outside the area marked in grey are mainly caused by the large scatter of the measured humidity values at −70 °C (see Fig. 8e).

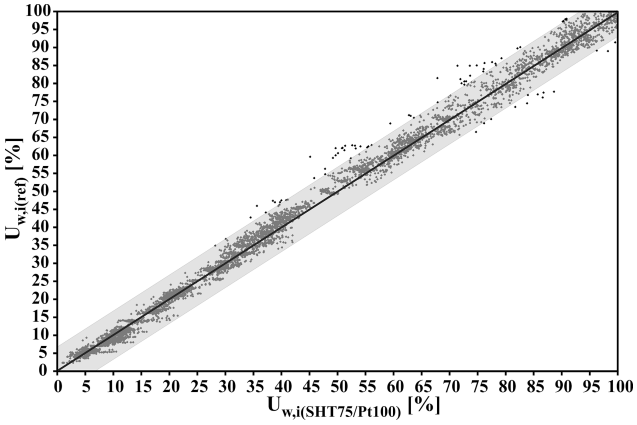

Figure 10. All measurements at all temperatures; the area marked in grey is the confidence interval (±7 %) of $U_{\mathrm{w,i}(SHT75/Pt100)}$ calculated with Eqs. (6)–(9) and $U_{\mathrm{w,i(ref)}}$ calculated with Eq. (5).

For fits with lower uncertainties, we recommend to calibrate the sensors for individual temperatures and/or pressures.

4 Conclusions

Pt100 and SHT75-sensors work reliably in the operating range given by manufacturer and the SHT75 even outside. The temperature measurement with SHT75 leads to significantly stronger variation of the measured values than with the Pt100 (Sect. 3.3). The comparison of the SHT75 humidity values with the reference humidity of the dew point

hygrometer shows a difference to the manufacturers fit at relative humidities below 20 % (see Sect. 3.4.1). The reason for this deviation remains unclear. The SHT75 shows a strong temperature dependency (Sect. 3.4.4) and also a pressure dependency below −10 °C (Sect. 3.4.3). No aging effects were observed (Sect. 3.4.2). A characteristic curve for the Pt100–SHT75 combination (Sect. 3.1.3) was calculated with an U_{99} of 7 % of the measured values (Sect. 3.4.4).

The experiment has demonstrated that it is possible to perform reliable humidity measurements at low vacuum and temperatures down to −70 °C using off-the-shelf sensors. The use of additional Pt100 instead of the SHT75 internal band-gap sensor is recommended for the reduction of measurement uncertainties. Moreover, characteristic curves should be recorded for each pressure, especially at temperatures < −20 °C (Sects. 3.4.3 and 3.4.4).

Further measurements of cross-sensitivity to other gases (e.g., CO_2), cf. Koncz et al. (2010), are necessary in order to validate these sensors for humidity measurements under extreme conditions such as a simulated Martian atmosphere.

Acknowledgements. Funding from German Federal Ministry of Economics and Technology – BMWi (project no. SF11021A) is gratefully acknowledged. I would like to thank David Wolter and Hendrik Hansen-Goos for many valuable suggestions and corrections to this manuscript.

Edited by: R. Maeda
Reviewed by: two anonymous referees

References

Bögel, W.: Neue Näherungsformeln für den Sättigungsdampfdruck des Wassersdampfes und für die in der Meteorologie gebräuchlichen Luftfeuchte-Parameter, 1977.

ECCOBOND 286: Data sheet: ECCOBOND® 286 A/B Easy Mix Ratio, General Purpose Epoxy Adhesive, 2013.

GUM: Bureau international des poids et mesures, Organització Internacional per a la Normalització, International Electrotechnical Commission, International Organization of Legal Metrology, 2008, Guide to the expression of uncertainty in measurement, International Organization for Standardization, Genève, 2008.

Hässelbarth, W.: BAM-Leitfaden zur Ermittlung von Messunsicherheiten bei quantitativen Prüfergebnissen, 2004.

Hudson, S. R., Town, M. S., Walden, V. P., and Warren, S. G.: Temperature, Humidity, and Pressure Response of Radiosondes at Low Temperatures, J. Atmos. Ocean. Tech., 21, 825–836, doi:10.1175/1520-0426(2004)021<0825:THAPRO>2.0.CO;2, 2004.

IST AG: Platinum Temperature Sensors: 6W – Product Series Temperature Range: −200 °C + 600 °C, 2012.

Koncz, A.: Entwicklung und Schaffung eines in-situ Feuchtemessgerätes für den Mars im Zusammenhang mit der ESA Marsmission ExoMars, Universität Stuttgart, Stuttgart, 2012.

Koncz, A., Lorek, A., and Wernecke, R.: Characterisation of capacitive humidity sensors under Martian pressure and temperatures down to −120 °C, in: Proceedings, MFPA Weimar, pp. 248–254, 2010.

Lorek, A. and Koncz, A.: Simulation and Measurement of Extraterrestrial Conditions for Experiments on Habitability with Respect to Mars, in: Habitability of Other Planets and Satellites, edited by: de Vera, J.-P. and Seckbach, J., Springer Netherlands, Dordrecht, 145–162, 2013.

Lorek, A., Koncz, A., and Wernecke, R.: Development of a gas flow independent coulometric trace humidity sensor for aerospace and industry, in: MFPA, MFPA Weimar, 289–296, 2010.

Miloshevich, L. M., Vömel, H., Paukkunen, A., Heymsfield, A. J., and Oltmans, S. J.: Characterization and Correction of Relative Humidity Measurements from Vaisala RS80-A Radiosondes at Cold Temperatures, J. Atmos. Ocean. Tech., 18, 135–156, doi:10.1175/1520-0426(2001)018<0135:CACORH>2.0.CO;2, 2001.

Sensirion AG: Datasheet SHT7x (SHT71, SHT75) Humidity and Temperature Sensor IC, 2011.

VDI/VDE 3514 Part 1: VDI/VDE 3514 Part 1: Measurement of humidity – Characteristics and symbols, 2007.

WMO: Technical Regulations Basic Documents No. 2 Volume I – General Meteorological Standards and Recommended Practices, World Meteorological Organization, Geneva, Switzerland, 2012.

Zent, A. P., Hecht, M. H., Cobos, D. R., Wood, S. E., Hudson, T. L., Milkovich, S. M., DeFlores, L. P., and Mellon, M. T.: Initial results from the thermal and electrical conductivity probe (TECP) on Phoenix, J. Geophys. Res., 115, 1–23, doi:10.1029/2009JE003420, 2010.